Reaction Chemistry & Engineering

ROYAL SOCIETY OF CHEMISTRY

PAPER

View Article Online
View Journal | View Issue

Cite this: *React. Chem. Eng.*, 2023, **8**, 2876

A novel process towards the industrial realization of large-scale oxymethylene dimethyl ether production – COMET†

Franz Mantei,[a] Christian Schwarz,[b] Ali Elwalily,[a] Florian Fuchs,[a] Andrew Pounder,[a] Hendrik Stein,[b] Matthias Kraume[c] and Ouda Salem *[a]

Oxymethylene dimethyl ethers (OME) show promising solubility and combustion properties for applications in various chemical processes and sectors. OME enable clean and quasi soot-free combustion, which can consequently lead to considerable NO_x emissions reduction. Besides reducing local emissions, OME can significantly reduce the global CO_2 emissions by substituting fossil diesel fuel if their production is based on sustainable methanol. Various process concepts for the OME production were proposed and investigated, but most of them have significant bottlenecks, which prevent their demonstration and scale-up in the near future. Only the production based on OME_1 and trioxane can already be demonstrated and scaled up, which, however, is complex and energy-intensive, considering a sustainable production based on H_2 and CO_2. Therefore, the novel COMET (clean OME technology) process concept is introduced and experimentally demonstrated utilizing only state-of-the-art process units. The COMET process relies solely on methanol and formalin as feedstock and overcomes the challenging water management aspect in the OME value chain, using a reactive distillation column. The COMET process is evaluated at a scale of 100 kilotons per annum OME_{3-5} product for the system boundary starting from H_2O electrolysis and CO_2 capture. Key performance indicators are defined and compared with alternative processes from the literature. The COMET process shows a high carbon efficiency of 88% and overall energy efficiency of 54% in comparison to the alternative OME_{3-5} production processes introduced in the literature. Moreover, the COMET process offers the forthwith large-scale production of OME in a relatively simple process chain and high technology readiness level.

Received 10th March 2023,
Accepted 26th July 2023

DOI: 10.1039/d3re00147d

rsc.li/reaction-engineering

1. Introduction

The fluctuating availability of renewable energies can be compensated by various measures, such as storage technologies like batteries and heat reservoirs. However, the need for long-term storage and long-distance transportation are met more easily and flexibly using power-to-X (PtX) technologies and products.[1] Green H_2 will play a key role in meeting these needs with already rising demands, as is suggested by various roadmaps, strategies, and international agreements by various governments and companies.[2,3]

Currently, fossil energy carriers are essential to provide heat and power, and are important carbon sources for the chemical, petrochemical and plastic industries. However, at the end of the life cycle, they are usually combusted to CO_2 which ends up in the atmosphere. Therefore, sustainable and circular carbon sources are required such as biogenic waste streams and CO_2 capture from air. One example of a circular carbon source is direct air capture (DAC) of CO_2. Due to its locally independent availability, DAC is experiencing a growing governmental interest with increasing numbers and capacities of technological demonstrations.[4]

A combination of captured CO_2 and green H_2 enables the implementation of these sustainable solutions into various sectors and hard to defossilize processes. One suitable product of CO_2 and H_2 are oxymethylene dimethyl ethers (OME). OME show promising fuel and physical properties for a wide range of potential applications such as solvents or diesel fuel additives or substitutes. OME_{3-5} have similar fuel properties to diesel fuel, a good solubility in diesel fuel and advantageous combustion behavior.[5,6] This makes OME

[a] *Sustainable Synthesis Products, Division Hydrogen Technologies, Fraunhofer Institute for Solar Energy Systems, Heidenhofstr. 2, 79110, Freiburg, Germany. E-mail: ouda.salem@ise.fraunhofer.de*
[b] *ASG Analytik-Service AG, Trentiner Ring 30, 86356 Neusäss, Germany*
[c] *Chair of Chemical Engineering, Technische Universität Berlin, Str. des 17. Juni 135, MAR 2-1, 10623 Berlin, Germany*

† Electronic supplementary information (ESI) available. See DOI: https://doi.org/10.1039/d3re00147d

attractive as a sustainable drop-in blending component for diesel fuel. Considering the high cetane number, OME can be an interesting dual fuel or ignition promoter in marine engines. Due to the absence of C–C bonds and the high amount of molecular bound oxygen, OME combust with distinct lower levels of emissions of particle matter than diesel fuel. Therefore, the NO_x and soot emission trade-off of diesel fuel can be avoided.[7,8]

The basis for large-scale sustainable production of OME is MeOH, which can be produced by reacting captured CO_2 with H_2 from renewable-powered H_2O electrolysis. Following this power-to-liquid (PtL) concept, the well-to-wheel (WtW) CO_2 emissions can be reduced by up to 93% compared to fossil fuels.[9,10] Furthermore, Voelker *et al.*[10] estimated an NO_x reduction of 57% and an almost complete reduction of soot using OME instead of diesel fuel. Moreover, small blending rates of OME in diesel fuel already show a clearly positive impact on global CO_2 emissions, as well as local NO_x and soot emissions.[10,11] With a worldwide demand of 26.5 million barrels diesel fuel per day,[12] small blending rates of OME showcase the need for large-scale production plants. Suitable compositions of the final OME_{3-5} product are defined by key properties, such as density, viscosity, cetane number and flash point, which are standardized in a new fuel pre-standard for OME DIN/TS 51699.[7,13]

Various process concepts have been proposed to produce OME from MeOH which will be discussed and compared in detail in the following sections. One of the main challenges of these processes, in terms of technical feasibility and energy demand, is the separation of the by-product H_2O from the target OME fraction. This H_2O is formed in various synthesis steps from MeOH to OME. The OME production processes discussed in the literature use different techniques to separate H_2O.[14–25] These techniques have different advantages and disadvantages, partly coupled with methods which are still in an early phase of investigation and demonstrations. In the present work, a new process concept, clean OME technology (COMET), is proposed which solves the challenging H_2O separation utilizing the state-of-the-art reactive distillation technique. This makes the COMET process a technically feasible process for large OME production capacities.

1.1. Objective of this work

The main objective of this work is the introduction of the novel COMET process concept for the production of OME from MeOH and aqueous formaldehyde (FA(aq.)) solutions, which solves the challenging H_2O management problem, using a reactive distillation column. Complementary, the experimental demonstration of the main COMET process units is introduced. The work further compares the COMET process concept major technical metrics to literature discussed OME production processes.

2. Theory and background

2.1. Synthesis of OME

OME are synthesized in an acidic environment from two methyl capping groups and n oxymethylene groups $–CH_2O–$. Suppliers for the methyl capping groups are methanol ($H_3C–OH$, MeOH), methylal ($H_3C–O–(CH_2O)_1–CH_3$, OME_1) or dimethyl ether ($H_3C–O–CH_3$, DME). For the oxymethylene groups, formalin (FA(aq.)), paraformaldehyde ($HO–(CH_2O)_n–H$ with n = 8–100, pFA) or trioxane ($(CH_2O)_3$, TRI) can be used.

In a solution of MeOH, FA, and H_2O, poly(oxymethylene) hemiformals ($HO–(CH_2O)_n–CH_3$ with n = 1–10, HF_n) and poly(oxymethylene) glycols ($HO–(CH_2O)_n–H$ with n = 1–10, MG_n) bound most of the FA, as described by eqn (1)–(4). These are fast reactions even in absence of a catalyst. The amount of monomeric FA in solutions with MeOH and H_2O is very small in chemical equilibrium.[26]

$$CH_2O + CH_3OH \rightleftharpoons HO(CH_2O)_1CH_3 \quad (1)$$

$$CH_2O + HO(CH_2O)_{n-1}CH_3 \rightleftharpoons HO(CH_2O)_nCH_3;\ n = 2–10 \quad (2)$$

$$CH_2O + H_2O \rightleftharpoons HO(CH_2O)_1H \quad (3)$$

$$CH_2O + HO(CH_2O)_{n-1}H \rightleftharpoons HO(CH_2O)_nH;\ n = 2–10 \quad (4)$$

HF_n are intermediate products for the production of OME. In an acidic environment HF_1 and MeOH react to OME_1 following the acetalization reaction described by eqn (5).

$$HO(CH_2O)_1CH_3 + CH_3OH \overset{H^+}{\rightleftharpoons} CH_3O(CH_2O)_1CH_3 + H_2O \quad (5)$$

The formation of $OME_{>1}$ follows a similar acetalization mechanism, as described by eqn (6), and a sequential addition or chain propagation mechanism, as described by eqn (7).[27]

$$HO(CH_2O)_nCH_3 + CH_3OH \overset{H^+}{\rightleftharpoons} CH_3O(CH_2O)_nCH_3 + H_2O;\ n = 2–10 \quad (6)$$

$$CH_2O + CH_3O(CH_2O)_{n-1}CH_3 \overset{H^+}{\rightleftharpoons} CH_3O(CH_2O)_nCH_3;\ n = 2–10 \quad (7)$$

By using TRI as a feedstock for the OME synthesis, three CH_2O units are formed in a first step, as described by eqn (8).

$$(CH_2O)_3 \overset{H^+}{\rightleftharpoons} 3CH_2O \quad (8)$$

$$HO(CH_2O)_3H \overset{H^+}{\rightleftharpoons} (CH_2O)_3 + H_2O \quad (9)$$

Furthermore, TRI can also be formed as a by-product following eqn (8), or by dehydration of MG_3, as described by eqn (9).[28]

Using DME as a feedstock for the OME synthesis, OME_1 is formed by the incorporation of FA into DME, as described by eqn (10).

$$CH_3OCH_3 + CH_2O \overset{H^+}{\rightleftharpoons} CH_3O(CH_2O)_1CH_3 \quad (10)$$

$$CH_3OCH_3 + (CH_2O)_3 \overset{H^+}{\rightleftharpoons} CH_3O(CH_2O)_3CH_3 \quad (11)$$

Furthermore, with DME and TRI as a feedstock for the OME synthesis, OME_3 is formed by direct incorporation of TRI into DME, as described by eqn (11).[29–31]

In addition to the main reaction network, side reactions lead to the formation of side products. Besides HF_n, MG_n, TRI and DME, the formation of tetroxane ($(CH_2O)_4$), methyl formate ($HCOOCH_3$, MEFO) and formic acid (HCOOH, FOAC) was observed, which strongly depends on the catalyst systems and increases with increasing temperatures.[32–34]

2.2. OME_{3-5} production processes

Different feedstock combinations can be used to produce OME_{3-5} due to various potential suppliers of methyl groups and oxymethylene groups. Depending on the formation of H_2O as a side product during the synthesis of OME_n, the reaction systems are classified as anhydrous or aqueous. Methyl group suppliers for anhydrous reaction systems are mainly DME and OME_1, because their conversion to OME_n only requires a chain propagation with oxymethylene groups, as described by eqn (7) and presented in Table 1. Oxymethylene group suppliers for anhydrous reaction systems are mainly TRI and monomeric FA, which do not contain H_2O or MeOH. Formalin, concentrated FA(aq.) or pFA contain H_2O and are used as oxymethylene group suppliers for aqueous reaction systems.

Feedstocks containing MeOH generally lead to the formation of H_2O as a side product in the aqueous OME synthesis, as described by eqn (5) and (6). This H_2O needs to be separated and extracted from the process loop to prevent accumulation. Fig. 1 shows a simplified scheme for the production of OME_{3-5} from various feedstocks. It consists mainly of a reactor for the OME synthesis R, two distillation columns CO-1 and CO-2 for product purification and a H_2O separation unit S for aqueous reaction systems. For the H_2O separation, various methods were proposed in the literature, such as extraction, adsorption or membrane, as discussed in the following section.

Various process concepts for the OME_{3-5} production were proposed in patents and other publications and some of them are realized in large-scale production plants in China. However, details regarding their performance, the quality and composition of the final OME product and the long-term operation are scarce.[35,36] Table 2 lists the main OME_{3-5} production processes discussed in the literature, emphasizing the feedstock, main advantages, and hurdles. A detailed description is provided in the ESI.† A comparison with the COMET process based on their performances in terms of OME_{3-5} yield, energy demand and technical feasibility is discussed in the results and discussion section. Further process concepts were proposed in the literature which show significant disadvantages in comparison to the process concepts presented in Table 2, as discussed in the ESI.†

Table 1 Methyl group suppliers and oxymethylene group suppliers for anhydrous and aqueous OME reaction systems

	Methyl group supplier	Oxymethylene group supplier
Anhydrous	DME, OME_1	TRI, monomeric FA
Aqueous	MeOH, DME, OME_1	FA(aq.), pFA, TRI, monomeric FA

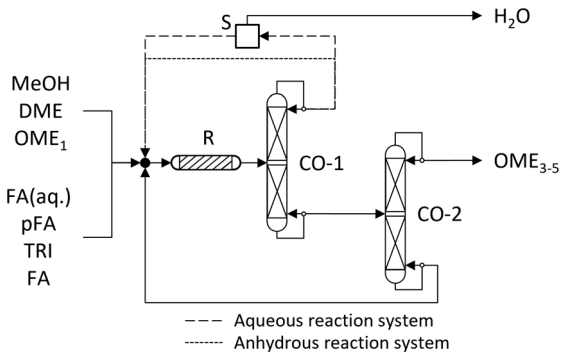

Fig. 1 OME_{3-5} production process for various feedstocks, following aqueous and anhydrous reaction systems. CO, distillation column; R, reactor; S, H_2O separator.

2.3. H_2O separation from the production of OME

One of the main challenging and energy-intensive process steps is the separation of the by-product H_2O from the production chain towards OME_{3-5}. Considering a sustainable production of OME_{3-5} based on MeOH produced from H_2 and CO_2, Fig. 2 shows how the synthesis of MeOH, intermediate products such as FA(aq.), DME and OME_1, as well as the synthesis of OME_n all result in the formation of H_2O.

In the MeOH synthesis from H_2 and CO_2, the OME_1 synthesis and the DME synthesis, H_2O is a by-product and separated using distillation columns.[19,37,38] In the partial oxidation of MeOH towards FA, as described by eqn (15), H_2O is formed as a by-product and used as a washing liquid in the absorber column. Downstream, H_2O is partly separated from FA(aq.) in a concentration step using evaporation techniques.[19,39] Therefore, H_2O is introduced into the TRI synthesis and separated in an energy-intensive cascade of distillation columns.[28,40] Only in the anhydrous FA synthesis, which is still in its very early stages, no H_2O is present.[41] Regarding the synthesis of $OME_{\geq 2}$, H_2O is not formed as a by-product when the oxymethylene group suppliers TRI or monomeric FA are combined with the methyl group suppliers DME or OME_1, as described by eqn (7) and (8).

This simplifies the final product purification. When starting from the cheaper and established reactant FA(aq.), H_2O will always be present in the OME_{3-5} sub-process and needs to be separated from the loop to circumvent accumulation. However, H_2O cannot be separated

Table 2 Advantages and main hurdles of various OME_{3-5} production process concepts

	Anhydrous synthesis			Aqueous synthesis		
Feedstock	OME_1 and TRI[14–16]	DME and TRI[17,18]	OME_1 and monomeric FA[19]	MeOH and FA(aq.)[20,21]	MeOH and monomeric FA[19]	OME_1 and FA(aq.) or pFA[19]
(+) Main advantages and (-) main hurdles	+ High OME_{3-5} yield after the synthesis	+ DME is cheaper than OME_1 [43]	+ High OME_{3-5} yield after the synthesis	+ Comparatively cheap feedstock	+ Comparatively cheap feedstock	+ Fairly high OME_{3-5} yield after the synthesis
	+ Simple product purification	- Complex and energy-intensive preparation of TRI[28,39,40,42]	+ Potentially simpler and cheaper production of monomeric FA	- Formation of H_2O as a side product	- Similar hurdles to MeOH and FA(aq.)	
	- Complex and energy-intensive preparation of TRI[28,39,40,42]	- High MEFO selectivity[29–31,44,45]	- Very low TRL of the monomeric FA production	- Low OME_{3-5} yield after the synthesis - Low TRL of the H_2O separation methods	- Very low TRL of the monomeric FA production	- Similar hurdles to MeOH and FA(aq.)

individually simply *via* distillation due to a complex phase behavior of the synthesis product mixture containing mainly FA, H_2O, MeOH, OME_{1-10}, HF and MG with several azeotropes with similar boiling points. The separation of H_2O from the loop is still a major challenge regarding the implementation of a potentially cheaper and scalable aqueous OME_{3-5} production process.

2.3.1. Extraction. Using an extractant for the separation of H_2O from the OME synthesis mixture separates the mixture into two phases, one organic phase mainly containing OME and the extractant and one aqueous phase mainly containing H_2O, FA and MG. Downstream to the extraction the organic phase can be separated and purified using distillation columns. The extractant is also separated and recycled back to the extraction. Various extractants were investigated in the literature showing that toluene, *p*-xylene and *n*-heptane enable promising liquid–liquid separation behaviors between OME and H_2O, FA and MG.[46–52]

Results of Li *et al.*[47] show the separation of the OME synthesis product using toluene. About 70% of OME are separated in the organic phase and only 14% of FA and H_2O migrate in the organic phase, as indicated by the split fraction. However, the organic phase mainly consists of toluene, which needs to be separated to be recycled. Furthermore, FA and H_2O still represent a large proportion of the organic phase and the aqueous phase still contains a large proportion of OME. A graphical illustration of the results of Li *et al.*[47] is presented in the ESI† in section 2.

An extraction method for the preparation of blends of OME in diesel fuel was proposed by Oestreich *et al.*[53] and discussed in the ESI.†

2.3.2. Adsorption. Schmitz *et al.*[20] investigated the adsorption of H_2O from a mixture containing FA, H_2O, MeOH and OME_{1-4} using zeolite 3A. Their results show that zeolite 3A has a good selectivity for H_2O with only small amounts of FA and MeOH being separated from the feed mixture. A graphical illustration of the results is presented in the ESI† in section 2. Ferre *et al.*[54] investigated the adsorption of H_2O using zeolite 3A from binary and ternary mixtures with MeOH and FA. Their results show that an increasing amount of FA or MeOH in the feed mixture leads to an increased adsorption of these components. However, the selectivity for H_2O is still far higher.

Regarding the separation of H_2O from an OME_{3-5} production process, the adsorption has the advantage of selectively separating H_2O from the loop, which enables the recycle of all other components to the OME synthesis. Due to the reaction network between H_2O and FA as described by eqn (3) and (4) not only the monomeric H_2O is separated, but also H_2O from MG_n. Therefore, a significant reduction of the overall H_2O content can be achieved. However, without H_2O, FA from MG_n remains in the mixture and either bounds with HF_{n-1} to long chain HF_n, or with MG_{n-1} to long chain MG_n or it remains in monomeric form. Either way, it increases the risk of local precipitations and, therefore, deactivation of the adsorbents. Therefore, a regeneration might be necessary. To reduce the risk of precipitation the temperature can be lifted, or the remaining H_2O content can be increased. The latter would, however, decrease the yield of OME_{3-5} in the OME synthesis and, therefore, increase the recycle streams and heat demand for separation. A suitable remaining H_2O content should be experimentally investigated and confirmed

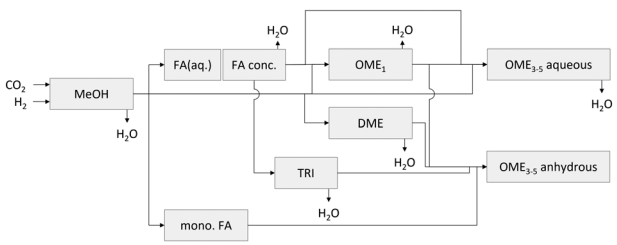

Fig. 2 H_2O separation from a sustainable production of OME_{3-5} based on H_2 and CO_2.

by long-term stability tests with alternating sequences of adsorption and regeneration. Furthermore, the scale-up potential should be investigated to ensure its feasibility for large-scale production plants.

Regarding the heat demand for the separation of H_2O *via* adsorption, Schemme *et al.*[43,55] estimated that 2.1 kW h kg^{-1} H_2O are required. Their estimations are based on the results from Schmitz *et al.*[20,56] and assume that the adsorbents are heated up from 25 °C to 235 °C for the regeneration using high pressure steam. Furthermore, it was assumed that the heat demand is mainly based on the heat of adsorption and the heat capacity of the adsorbents.

2.3.3. Membrane. Schmitz *et al.*[57] tested two zeolite membranes type NaA and type T from Mitsui & Co. as well as three PVA-based polymer membranes PERVAP 4100, PERVAP 4101 and PERVAP 4102 from DeltaMem AG for a mixture containing FA, H_2O, MeOH, OME_1 and OME_2. Their results show that the zeolite membranes and the PERVAP 4102 were not suitable for the separation task, while the PVA-based polymer membranes PERVAP 4100 and PERVAP 4101 could separate H_2O with a high selectivity, also for the repeated experiment with the tested zeolite membranes. A graphical illustration of the results by Schmitz *et al.*[57] using the PERVAP 4100 membrane is presented in the ESI† in section 2.

However, Ferre *et al.*[58] reported the application of a different membrane from DBI Gas und Umwelttechnik. The long-term stability of the membrane, selectivities in the reaction mixture and the scale-up potential should be further investigated to ensure its feasibility for large-scale production plants.

The advantages of the membrane for the separation of H_2O are similar to the advantages of the adsorption with a high selectivity for H_2O. However, likewise to the adsorption, this results in a higher risk for local precipitation. Therefore, a compromise might be necessary between the long-term stability and the H_2O concentration of the retentate. A disadvantage of a higher H_2O concentration in the retentate is an increase of the recycle streams which results in higher heat demands for the product purification and reduces the overall energy efficiency of the process.

Regarding the heat demand for the separation of H_2O *via* membranes, Held *et al.*[39] estimated that 0.7 kW h kg^{-1} H_2O are required. This results from the evaporation of H_2O after passing through the membrane to the reduced pressure of the permeate of 0.03 bar. Held *et al.*[39] assumed that no external heat is required but the temperature of the process stream is reduced from 84 °C to 36 °C. In comparison to the separation of H_2O *via* adsorption, the heat demand is significantly lower.

Table 3 summarizes the main advantages and main hurdles of the H_2O separation methods extraction, adsorption, and membrane.

Table 3 Main advantages and main hurdles of the H_2O separation methods extraction, adsorption, and membrane

Method	Extraction	Adsorption	Membrane
H_2O selectivity	Low	High	High
Energy demand	High	High	Comparatively low
Long-term operation	Likely	Challenging	Challenging
Scale-up potential	Likely	Challenging	Challenging

3. COMET process description

The COMET process[59] is based on the commercially available MeOH and FA(aq.) feedstock and produces mainly high purity OME_{3-5}, as illustrated in Fig. 3. For the separation of H_2O from the loop, a reactive distillation column is used.

The COMET process starts at the concentration of 50–55 wt% FA(aq.) (stream 1), which can be the product stream of a state-of-the-art FA production process.[19,60] The stream is mixed with the distillate of the second evaporator E-2 and the bottom of the third evaporator E-3. The FA(aq.) is then concentrated in a cascade of two evaporator stages E-1 and E-2 to provide a concentrated FA(aq.) of 85–88 wt% FA (stream 5) and an aqueous stream containing 10–25 wt% FA (stream 3). The concentrated FA(aq.) (stream 5) is used for the production of OME and mixed with the recycle streams, containing the azeotropic mixture of OME_1 and MeOH (stream 10) and $OME_{\geq 6}$ (stream 14). The mixture is converted in a fixed bed reactor R filled with an acidic heterogeneous catalyst. In contrast to the OME production process based on MeOH and FA(aq.),[20] the reactor inlet stream contains mainly OME_1 as a methyl capping source. This improves the selectivity towards OME_{3-5}. The comparatively high selectivity further increases with decreasing H_2O and MeOH concentrations in the concentrated FA feedstock (stream 5) and OME_1 recycle (stream 10). The synthesis product mixture, mainly containing FA, H_2O, MeOH and OME_{1-10} (stream 7), is separated in a cascade of three distillation columns. In the first distillation column CO-1, $OME_{\geq 3}$ are separated from the more volatile components FA, H_2O, MeOH and OME_{1-2}. Importantly, OME_3 cannot be completely separated to the bottom product, a small fraction remains in the distillate. In the third distillation column CO-3, $OME_{\geq 6}$ are separated and recycled to the reactor and a final product mixture (stream 13) of OME_{3-5} is withdrawn at the top of CO-3. The distillate product of CO-1 is mixed with MeOH (stream 9) and sent to a reactive distillation column CO-2, to separate an azeotropic mixture of OME_1 and MeOH (stream 10) from FA and H_2O (stream 11). On the catalytic trays, two main conversions take place. First, OME_2 and OME_3 are converted to OME_1 and FA over an acidic heterogeneous catalyst, as described by eqn (7). In addition, MeOH and FA are converted to OME_1 and H_2O, following the acetalization reaction as described by eqn (1) and (5). The mechanism on the catalytic trays is illustrated in Fig. 4. Due to the evaporation and, therefore, the separation of the volatile product OME_1 from the liquid reaction mixture, the equilibrium of eqn (5) and (7) shifts, and the reactions proceed towards the production of OME_1. Therefore, with sufficient retention time, OME_2 is converted

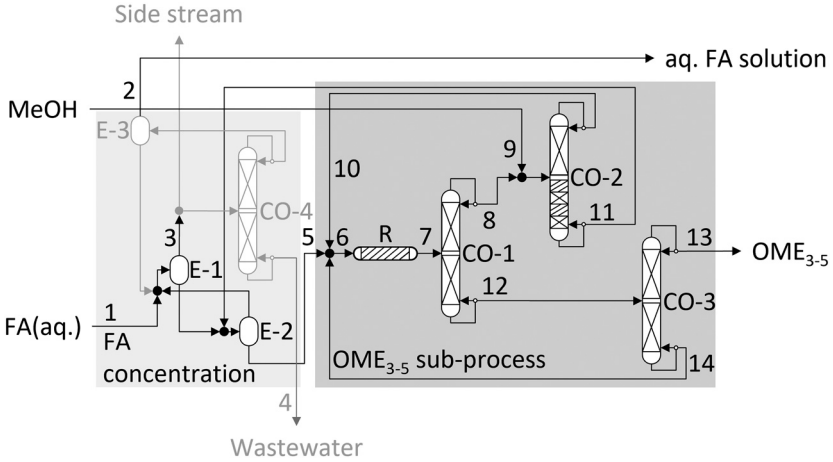

Fig. 3 COMET process concept for the production of OME_{3-5} from MeOH and FA(aq.) feedstocks. The light grey arrows and process units were added in this work to the FA concentration sub-process to improve the recycle of FA. CO, distillation column; E, evaporator; R, reactor.

to a large extent to OME_1, while the conversion of FA towards OME_1 is limited by the amount of MeOH. The mixture is separated into the azeotropic mixture of OME_1 and MeOH in the distillate (stream 10) and a mixture of FA and H_2O in the bottom (stream 11). The distillate product of CO-2 is recycled back to the reactor and the bottom product is recycled to the evaporator E-2 for the FA concentration to separate H_2O from the process and recycle concentrated FA back towards the OME reactor. Therefore, the reactive distillation column prevents the accumulation of H_2O inside the loop and solves the challenging H_2O management. In contrast to the H_2O separation from the loop using adsorption or membranes, in the COMET process H_2O is not separated selectively but together with the remaining FA. This significantly reduces the risk of precipitation, since enough H_2O is left to convert the remaining FA to comparatively short-chain MG_n which stay liquid at elevated temperature for sufficient retention time to downstream processing steps.

A similar concept for a reactive distillation column is applied in the OME_1 production process by Drunsel *et al.*[61,62] with the purpose to achieve a complete conversion of FA after the OME_1 reactor.

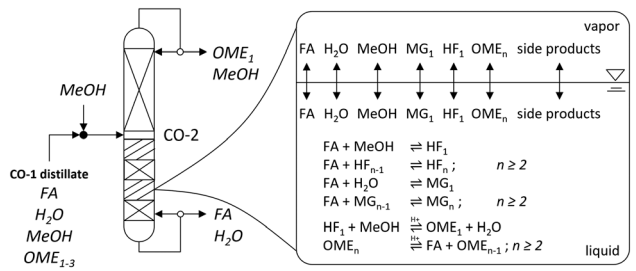

Fig. 4 H_2O separation from the COMET process *via* reactive distillation. The left side shows the reactive distillation column with the main components of the feed and product streams. The illustration on the right side shows the interaction on a catalytic tray and was adopted from Schmitz *et al.*[56]

The amount of MeOH (stream 9) added to the feed of the reactive distillation column CO-2 defines the conversion of FA and oxymethylene groups with MeOH on the catalytic trays towards OME_1, following eqn (1), (5) and (7). Therefore, a variation of the amount of MeOH (stream 9) varies the amount of OME_1 produced as the distillate product of the reactive distillation column CO-2. For the OME synthesis in the fixed bed reactor R a constant ratio of OME_1 to concentrated FA(aq.) is required before the reactor. Therefore, the amount of MeOH (stream 9) can be defined to exactly produce the amount of OME_1 required for the OME synthesis. Or the amount of MeOH (stream 9) can be increased to produce more OME_1 than required by the OME synthesis and the excess OME_1 can be extracted as a by-product. Another advantage of the COMET process is that the process offers a tunable product portfolio of OME. In the present work the amount of MeOH added to the reactive distillation column CO-2 was limited to only produce the required amount of distillate product (stream 10) for the OME synthesis and, therefore, achieve higher OME_{3-5} selectivity. Considering the production of OME_1 as a target side product of the COMET process, another distillation column can be added to achieve high purities of the OME_1 side product, similar to the second distillation column of the production process for OME_1.[61]

Besides the OME_{3-5} product (stream 13), wastewater (stream 3) is produced with FA concentrations of about 10–25 wt%. This by-product stream is not limited to the COMET process but part of all OME_{3-5} production processes using FA(aq.) as an intermediate product. Instead of its disposal and to increase the carbon yield of the process, several strategies are possible to handle this stream. In the present work, the stream was partly send to the absorber column of the FA(aq.) production and concentrated in an additional distillation column CO-4. The concentrated FA stream was further concentrated in another evaporator E-3 to recycle the concentrated FA stream and to separate the stream with a low FA concentration (stream 2). This stream is also the purge stream for traces of MeOH and other volatile

components to avoid accumulation in the loop. Instead of its disposal, this stream can be used to dilute an FA(aq.) product stream to prepare a stable formalin product.

3.1. Expanding the system boundary starting from H_2 and CO_2 feedstocks including the intermediate production of FA and MeOH

To enable a consistent basis of comparison with alternative OME_{3-5} production processes, the system boundary is extended to account for a sustainable OME_{3-5} production based on green H_2 and captured CO_2. The intermediate production of MeOH and FA(aq.) is described in detail by Mantei *et al.*[19] A simplified process flow diagram of the extended COMET process concept starting from H_2 and CO_2 is illustrated in Fig. 5. The MeOH production starts from the compression of the feedstock H_2 and CO_2, the mixing with the recycle stream, and the synthesis of MeOH, as described by eqn (12)–(14).

$$CO_2 + 3H_2 \rightleftharpoons CH_3OH + H_2O \quad (12)$$

$$CO_2 + H_2 \rightleftharpoons CO + H_2O \quad (13)$$

$$CO + 2H_2 \rightleftharpoons CH_3OH \quad (14)$$

The synthesis product is purified in a cascade of two phase separators followed by a distillation column to prepare high purity MeOH. Part of the MeOH is used for the synthesis of FA. Therefore, MeOH and H_2O are mixed with the recycle stream and air for the conversion to FA, as described by eqn (15)–(17).

$$CH_3OH + \frac{1}{2}O_2 \rightarrow CH_2O + H_2O \quad (15)$$

$$CH_3OH \rightleftharpoons CO + 2H_2 \quad (16)$$

$$CO + \frac{1}{2}O_2 \rightleftharpoons CO_2 \quad (17)$$

The synthesis product is purified in an absorber column to separate FA and H_2O from H_2, CO, CO_2 and N_2 using part of the wastewater from the FA concentration as a washing liquid. The product mixture of FA and H_2O is concentrated in the FA concentration sub-process, as described in the previous section.

To use the heating value of the purge streams, a combustion sub-process was implemented. Following the assumptions from Mantei *et al.*,[19] excess air was added to achieve complete combustion and keep the adiabatic temperature rise below 800 °C. The stoichiometric amount of O_2 required for a complete combustion is described by eqn (18).

$$C_xH_yO_z + \frac{1}{2}(2x + 1/2y - z)O_2 \rightarrow xCO_2 + \frac{1}{2}yH_2O \quad (18)$$

4. Materials and methods

4.1. Experiments

4.1.1. Chemicals and materials. The reactants OME_1 (purity > 99.8%) and MeOH (purity > 99.8%) were purchased from Brenntag GmbH and provided from ChemCom Industries B.V. The reactant FA(aq.) was provided as a stabilized aqueous FA (approx. 37 wt%) solution with low amounts of MeOH (≤0.5 wt%) by ChemCom Industries B.V.. The catalyst Amberlyst® 46 (A46) was provided by INAQUA Vertriebsgesellschaft mbH. Ion exchange resin (IER) III was purchased from Merck Chemicals GmbH.

4.1.2. Analysis. The samples were analyzed by ASG Analytik-Service AG. The FA content was determined by the sodium sulfite method for concentrations higher than 0.2 wt% and by voltametric analysis for smaller concentrations.[63] The H_2O content was determined by Karl-Fischer titration. The content of OME_{1-10}, MeOH, TRI, tetroxane and MEFO was determined by a gas chromatographic method using flame ionization detection (GC-FID). An online GC equipped with a thermal conductivity detector (GC-TCD) was used for online measurements. The applied methods for the GC analysis were ASG 2506 GC-FID for the organic compounds and ASG 2504 GC-FID for TRI and tetroxane.

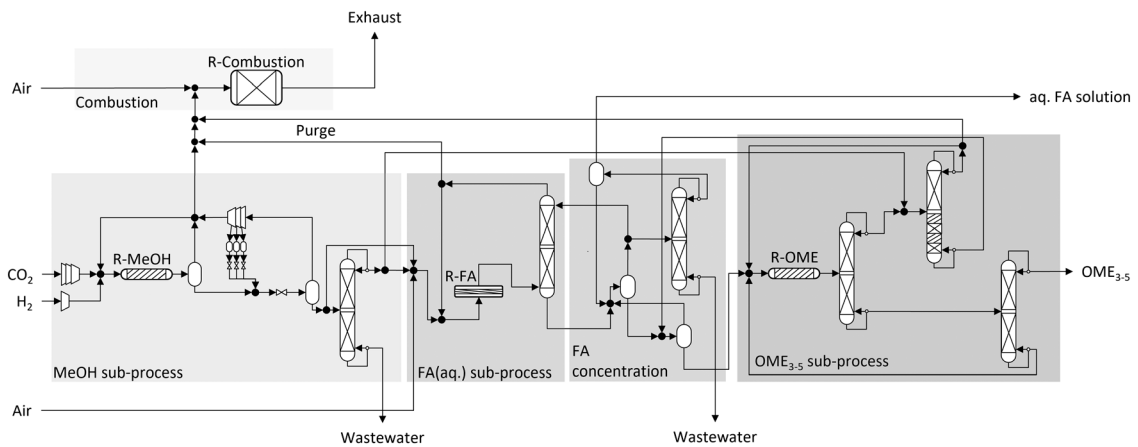

Fig. 5 COMET process concept for the production of OME_{3-5} from H_2 and CO_2 feedstock with the intermediate production of MeOH and FA.

4.2. Experimental setups

4.2.1. Concentrated FA(aq.) feed preparation. A cascade of two thin film evaporators was used to provide the concentrated FA(aq.) solution. The setup was provided and operated by VTA Verfahrenstechnische Anlagen GmbH & Co. KG and directly connected to the OME synthesis setup. As a preparation, the stabilized FA(aq.) containing about 37 wt% FA was concentrated to about 55 wt% FA, which is the typical concentration of the product of a conventional FA(aq.) production plant. The product was stored in a heated tank and further concentrated prior further concentration. Two concentration steps followed. In a first step the FA(aq.) was concentrated to about 75 wt% FA and in a second step to about 85–89 wt% FA. The evaporators were operated under vacuum at about 200–600 mbar and temperatures of the heating fluid of 100–150 °C. A simplified process flow diagram is illustrated in Fig. S9 in the ESI.†

4.2.2. OME synthesis. For the synthesis of OME, a fixed bed reactor with a capacity of 1–5 L h^{-1} was used. The setup contains a pump and heat exchanger to pressurise and heat up the reactant OME_1 to meet the synthesis conditions, as well as a pump and heated tubes for the concentrated FA(aq.) from the thin film evaporators. After mixing the reactants, the stream was converted in a fixed bed reactor filled with the IER catalyst A46 and heated to about 90 °C. The synthesis product was mixed with additional MeOH, cooled to ambient temperature, depressurized, and directly analyzed using the GC-TCD before it was stored at room temperature. A simplified process flow diagram is illustrated in Fig. S10 in the ESI.†

Before using the catalyst A46, it was stored in a mixture of FA, H_2O, MeOH and OME_1 to prevent further swelling inside the reactor unit.

The addition of MeOH to the OME synthesis product allowed for a stable storage and transport. The stabilization was a preventive measure to ensure a homogeneous liquid solution without precipitation even at low temperatures and long storage periods. The amount of additional MeOH was determined to meet the demand for the reactive distillation column in an integrated process, see Fig. 3 and the description in section 3. The targets of the reactive distillation column were a bottom product with a concentration of about 60 wt% FA and H_2O, as well as an almost complete conversion of MeOH. The latter target assumes that OME_{2-3} are converted to FA and OME_1 as described by eqn (7), MeOH and FA are converted to OME_1 and H_2O as described by eqn (1) and (5), and the distillate product is the azeotropic mixture of OME_1 and MeOH at ambient pressure.

4.2.3. OME synthesis product neutralization. The OME synthesis product was pumped through a neutralization bed of IER III at ambient temperature and stored prior to the thermal separation in the distillation column.

4.2.4. Thermal separation in CO-1. A DN50 glass distillation column with one upper and one lower section of 70 cm height each was used for all thermal separation steps.[64] For the investigation of the first separation step in CO-1, the two sections of the column below and above the feed were filled with Montz 750 structured packings. A horizontal reboiler was used which prevented the flooding of the column in the start-up phase due to strong foaming of the mixture at boiling conditions. The column was continuously operated at ambient pressure with a feed rate of 1–2 L h^{-1} for about 250 kg OME synthesis product for about 200 h. After achieving steady state, distillate and bottom products were withdrawn continuously from the column. A simplified process flow diagram is illustrated in Fig. S11 the ESI.†

4.2.5. Reactive distillation in CO-2. The core step of the COMET process concept takes place in CO-2. The distillate product of CO-1 was used as the feedstock for CO-2. The same distillation setup of CO-1 was used for the experimental investigation of the reactive distillation CO-2. The lower section of the column was filled with a fixed bed of the catalyst A46 and Montz 750 structured packing on top. The upper section above the feed was filled with Montz 750 structured packing. The column was continuously operated at ambient pressure with a feed rate of 0.5–1 L h^{-1} and for about 150 kg feedstock under continuous withdrawal of distillate and bottom product at steady state conditions.

4.2.6. Thermal separation in CO-3. The bottom product of CO-1 containing mainly $OME_{\geq 3}$ was fractionated in CO-3. The same distillation setup of CO-1 was used for the experimental investigation of the thermal separation in CO-3 with Montz 750 packings in the upper and lower sections. The setup was continuously operated at about 100 mbar with a feed rate of 2–3 L h^{-1} and for about 50 kg feedstock under continuous withdrawal of distillate and bottom product at steady-state conditions.

4.3. Process simulation and evaluation

4.3.1. Process modelling and simulation. The process simulation software Aspen Plus® V12 was used for the steady-state simulation of the COMET process based on H_2 and CO_2. Aspen Energy Analyzer V12 was used for heat integration.

The components H_2, CO_2, CO, N_2, O_2, FA, MeOH, H_2O, OME_{1-10}, HF_{1-10} and MG_{1-10} were considered. The properties for OME_{2-10}, HF_{1-10} and MG_{1-10} were not included in the Aspen database. Their properties were introduced as new components according to a previous work of our group.[19] The rest of the components properties were adopted from Aspen database. Details are described by Mantei *et al.*,[19] who also describe the UNIFAC-based model which was used as a basis for the process simulation.

Pressure values presented in this work describe the absolute pressure.

The methodology for the process simulation including the individual simulation of all sub-processes, the material integration and interconnection, convergences, the

adjustment of the production capacity and finally the heat integration followed the procedure from Mantei *et al.*[19]

For the simulation of the reactive distillation column, the kinetic model from Schmitz *et al.*[27] for the OME synthesis over A46 for feedstocks comprising MeOH, FA, H_2O and OME_1 was used. The model was implemented in a Fortran subroutine and activated on the catalyzed trays inside the RadFrac column. The implementation of the kinetic model was validated with the experimental results from Drunsel,[61] who investigated a reactive distillation column in the OME_1 production process for a similar reactive separation task, however, using the catalyst A15 instead of A46. A good agreement was obtained between experimental and simulation results. Furthermore, the subroutine was slightly adjusted to be used in a reactor unit and was validated with the experimental results from Schmitz *et al.*[27] with a good agreement. In contrast to the kinetics of the OME formation as described by eqn (5)–(7), the model assumes the formation of HF_n and MG_n as described by eqn (1)–(4) to be in chemical equilibrium at all retention times.

Regarding the side products HF_n and MG_n for mixtures containing FA, H_2O and MeOH, the true composition was used for the process simulation, which considers the presence of HF_n and MG_n. The overall composition, considering the stoichiometric decomposition of HF_n and MG_n to their reactants MeOH, H_2O and FA, was used for the evaluation and the presentation of the results.

The formation of the side products TRI, DME, MEFO, FOAC and tetroxane was not considered in the process simulation, due to very small concentrations in the synthesis product when A46 is used as a catalyst.

4.3.2. Process evaluation and comparison criteria. The COMET process was evaluated using various key performance indicators (KPIs). This allows a consistent basis of comparison with other OME_{3-5} production processes which are described by Mantei *et al.*[19] Therefore, the same equations were used to determine the process energy efficiency, carbon efficiency and the material selectivity, as described by eqn (19)–(21).

$$\eta_{\text{energy}} = \frac{\dot{m}_{\text{OME}_{3-5}} \cdot \text{LHV}_{\text{OME}_{3-5}}}{\sum_k \dot{Q}_k + \sum_l W_l + \sum_i \dot{m}_i \cdot \text{LHV}_i} \tag{19}$$

$$\eta_{\text{C}} = \frac{C_{\text{OME}_{3-5}}}{\sum_i C_i} \tag{20}$$

$$\eta_{\text{mass}} = \frac{\dot{m}_{\text{OME}_{3-5}}}{\sum_i \dot{m}_i} \tag{21}$$

where $\dot{m}_i$ denotes the mass flow rate of the reactants i, LHV denotes the lower heating value at 298 K, $\dot{Q}_k$ and W_l represent the externally supplied heat flows and electric power and C denotes the number of carbon atoms.

5. Results and discussion

5.1. Experimental demonstration

In the following sections the experimental results of the demonstration of the main COMET process units are presented and discussed. All investigations were carried using state-of-the-art experimental setups. The FA concentration units and the OME synthesis unit were interconnected. The products were collected and subsequently further processed in the distillation units.

5.1.1. OME synthesis. The continuous OME synthesis was investigated experimentally by feeding pure OME_1 and a concentrated FA(aq.) solution in a fixed bed reactor with 2.7–3.5 L h^{-1} at about 90 °C and 10 bar over the catalyst A46. Fig. 6 illustrates the composition of the feed mixture (F), the simulated equilibrium product composition (P-Sim), two preliminary experimental products (P1–2-Exp) from the starting phase and the three product barrels (P3–5-Exp) which contained about 250 kg of the OME synthesis product.

The compositions of the three product barrels (P3–5-Exp) show a good agreement with the simulated equilibrium composition (P-Sim). Comparing the three product compositions among each other, a small shift towards longer chain $OME_{\geq 3}$ and FA with increasing time on stream was observed. This is mainly a result of the slightly fluctuating FA concentration in the concentrated FA(aq.) feed stream (85–88 wt% FA) from the evaporation units and the feed stream flowrates. The OME_1 flowrate was regulated to meet a constant ratio between OME_1 and FA, while the FA flowrate was regulated to stabilize the level of the small storage between the second thin film evaporator and the OME synthesis sub-process. Although there was good agreement of the chemical equilibrium between simulation and experiment results, the kinetics of the OME synthesis were predicted to be much faster than those found experimentally. The simulation predicted the chemical equilibrium at a weight hourly space velocity (WHSV, feed mass flow in

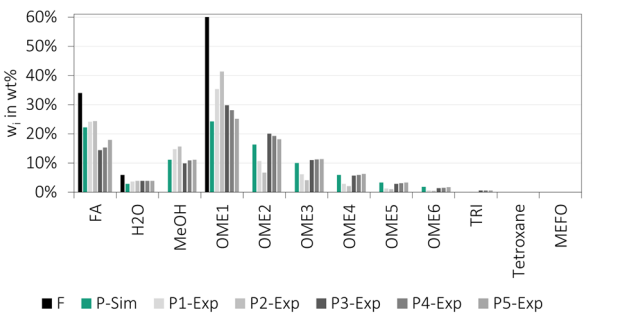

Fig. 6 OME synthesis from OME_1 and concentrated FA(aq.) over A46 (conditions: concentrated FA(aq.) with 85–89 wt% FA, (concentrated FA(aq.))/OME_1 = 0.6 g g^{-1}, A46/(OME_1 + concentrated FA(aq.)) = 0.34 g g^{-1} h^{-1}, approx. 3 L h^{-1}, 90 °C, 10 bar, fixed bed reactor). F represents the feed composition. P-Sim, P1–5-Exp represent the product composition of the simulated equilibrium, two experimental preliminary products P1–2 from the starting phase and the three product barrels P3–5, respectively.

relation to the amount of catalyst) of about 70 h^{-1}. However, the experiments were carried out at a WHSV of approximately 16 h^{-1} and 3 h^{-1}, whereby only the lower WHSV was sufficient to obtain chemical equilibrium, as presented by P3–5-Exp in Fig. 6. The WHSV of 16 h^{-1} led to high amounts of unreacted FA, low concentrations of $OME_{\geq 3}$ and, therefore, solidification of the synthesis product after cooling and without adding MeOH for stabilization, as presented by P1–2-Exp in Fig. 6. The kinetic model from Schmitz *et al.*[27] was used for the simulation, which was initially regressed on experimental results of the OME synthesis from MeOH and FA with partly higher concentrations of H_2O or OME. Therefore, the feed mixture already contained high concentrations of HF which can directly react to OME, as described by eqn (5) and (6). Furthermore, the model was based on the assumption that the reactions towards HF and MG, as described by eqn (1)–(4), are in equilibrium at all retention times since their kinetics are much faster than the kinetics of the formation of OME. In the COMET process this assumption is not met. The concentration of MeOH in the feed is very low because OME_1 was used as methyl group supplier instead. Therefore, FA is bound mainly in MG which need to depolymerize to be converted to OME, as described in the ESI† in the section about the OME_{3-5} production process based on OME_1 and FA(aq.) or pFA. This is the limiting step for the reaction kinetics of the COMET process but not significant for the OME synthesis based on MeOH and FA. Therefore, the kinetic model[27] is a suitable basis but needs to be further extended to realistically describe the reaction progress of other feed mixtures, which is required to correctly design the reactor unit.

Besides the main components, small fractions of the side products MEFO, TRI and tetroxane were detected in the product barrels P3–5 of about 0.1 wt%, 0.6 wt% and 0.1 wt%, respectively. For P1–2 (during the starting phase) concentrations of about 0.1 wt%, 0.1 wt% and 0.03 wt% were obtained. Therefore, these concentrations strongly depend on the WHSV, which is a matter of investigation for high yields of OME_{3-5} at low concentrations of the side product.

5.1.2. Synthesis product neutralization. Before the separation of the OME synthesis products P3–5 in the continuous distillation setup, the thermal stability was tested with a similar procedure to the investigations from Mantei *et al.*[33] The pre-tests were conducted in a micro distillation setup using about 50 mL of P3–5 with a stepwise increase of the reboiler temperature. The distillation led to a solidification of the bottom products for all three samples. However, while P3 solidified at about 130 °C, P4 only solidified at about 170 °C and P5 solidified only after heating up to 170 °C and cooling down the bottom product. Additionally, the electric conductivity was measured for the three samples with a reduction from 6.3 μS cm^{-1} for P3, 3.2 μS cm^{-1} for P4 and 2.1 μS cm^{-1} for P5. This indicates that the reduced thermal stability of the OME synthesis product is an initial phenomenon. Nevertheless, for the thermal separation of P3–5 a neutralization was necessary. Further pre-tests were conducted with different retention times of the IER III in the OME product mixtures for neutralisation. The results indicated that a WHSV of about 12 h^{-1} was sufficient to neutralize the OME synthesis product at ambient temperature. This WHSV includes a high safety margin and can probably be increased, especially for the OME synthesis product after longer times on stream of the catalyst. Furthermore, the results showed a connection between the thermal stability of the synthesis product as verified by the micro distillation and the electric conductivity. Below an electric conductivity of 0.2 μS cm^{-1} the synthesis product was thermally stable, and the distillation did not change the product composition. Above 1.0 μS cm^{-1} changes in the composition were detected. Finally, the OME synthesis product of the three product barrels P3–5 was neutralized at ambient temperature in a fixed bed of IER III at a WHSV of about 12 h^{-1} using about 500 g IER III. A deactivation of the IER III with increasing time on stream was not observed for the OME synthesis product, of about 200 kg which was continuously neutralized in the fixed bed.

During the investigation of the OME synthesis for about 80 h on stream, stable catalytic activity was observed. Also under reactive distillation conditions, the catalyst performance did not show an obvious deactivation for about 600 h on stream. However, further investigations are required to verify if the changing thermal stability is an initial phenomenon of the catalysts time on stream. In addition to the impact on the process design, the cause of this behavior should be further investigated. It might only be the leaching of the catalyst as emphasized by Fink *et al.*[65,66] and Baranowski *et al.*,[67] but it could also be influenced by the side product formation, especially formic acid, which was not analyzed in this work but reported in the literature.[32]

5.1.3. Synthesis product separation in CO-1. After the neutralization of the OME synthesis products P3–5, the distillation of the volatile components FA, H_2O, MeOH and OME_{1-2} from $OME_{\geq 3}$ was investigated in the distillation setup. The results illustrated in Fig. 7 are an example but representative result of the continuous distillation

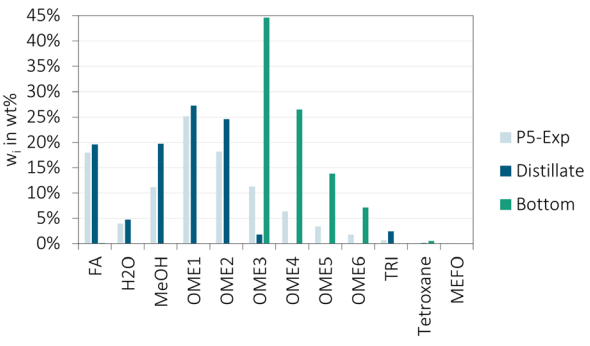

Fig. 7 CO-1, OME synthesis product separation (conditions: 2 L h^{-1}, reflux/distillate = 0.5–2 s s^{-1}, distillate/feed = 81 wt%, Montz 750 structured packing, 85–175 °C, ambient pressure). The values describe the mass fractions of the feed mixture, here P5-Exp as presented in Fig. 6, the distillate product and bottom product.

experiment and show that the targeted separation between OME_2 and OME_3 was successfully realized. It also shows that FA, H_2O and MeOH can be separated from $OME_{\geq 3}$. The side products MEFO and TRI are also separated from the bottom product, but the side product tetroxan has a higher boiling point than OME_3 and stays in the bottom product.

The distillation setup was operated at a feed temperature of 87 °C, a condensation temperature of 85 °C and a reboiler temperature of 175 °C. The distillate to feed ratio was about 0.81 and the time-based reflux ratio was varied as a controlled variable between 0.5–2 s s^{-1} (time controlled) to achieve a constant condensation temperature.

Fig. 7 shows that OME_2 was completely separated to the distillate product. However, also a small fraction of OME_3 went to the distillate product, which was about 14% of the feed amount of OME_3. Besides $OME_{\geq 3}$, traces of FA, H_2O and MeOH were detected in the bottom product which were mainly below 0.6 wt%. MEFO was not detected in the bottom product.

Regarding the continuous operation of the distillation setup, an increasing precipitation of FA inside the condenser was challenging in the initial phase but could be prevented by increasing the temperature of the cooling fluid to above 25 °C. However, as a result the temperature difference decreased between the cooling fluid and the boiling points of the most volatile components MEFO, the azeotropic mixture of OME_1 and MeOH, as well as OME_1. Thus, the area of the condenser was relatively small to obtain a complete condensation and a small fraction of the most volatile components accumulated in a cool trap. As a result, the ratio of OME_1 to OME_2 in the feed mixture P5-Exp differs from the ratio of OME_1 to OME_2 in the distillate product.

5.1.4. Reactive distillation in CO-2. After the separation of the OME synthesis product in CO-1, the distillate product of CO-1 was separated and converted in a reactive distillation column CO-2.

A representative result of the continuous reactive distillation experiment is illustrated in Fig. 8. The distillate and bottom product compositions show that the targets of the reactive distillation column were obtained. $OME_{\geq 2}$ were converted to OME_1 and FA, the composition of the distillate product is the azeotropic mixture of OME_1 and MeOH and the bottom product contains mainly FA and H_2O. Regarding the bottom product composition, small concentrations of MeOH of about 0.3 wt% were detected besides the desired range of FA and H_2O. Furthermore, traces of OME_{1-6} were detected with concentrations far below 0.1 wt%. However, as a result of the high H_2O and FA content in the bottom product, the quantification of traces is complex due to the fast precipitation of the bottom product solidifies fast if not heated or diluted.

CO-2 was operated at a condensation temperature of 45 °C and reboiler temperature of 104 °C with a distillate to feed ratio of about 0.63.

The results confirm that the reactive distillation column is a feasible instrument for the separation of H_2O from the OME_{3-5} production loop of the OME_{3-5} production and that an almost complete conversion of MeOH can be achieved. Furthermore, the results indicate, that the variation of the amount of MeOH in the feed mixture to the reactive distillation column can be used to tune the amount of OME_1 produced as the distillate product.

5.1.5. Product separation in CO-3. The representative results of the continuous distillation experiment for the separation of the final product mixture OME_{3-5} from the bottom product of the distillation column CO-1 are illustrated in Fig. 9. The target was a cut between OME_5 and OME_6. A significant amount of OME_5 stayed in the bottom product, which, however, can be separated to the distillate product by increasing the reboiler temperature or reducing the operational pressure. Regarding the distillate product, besides OME_{3-5}, small fractions of OME_6 of 0.2 wt%, tetroxan of 0.7 wt% and traces of FA and H_2O were detected. The concentration of tetroxan is mainly a result of the retention time, temperature, and selection of catalyst in the reactor, which can be improved to reduce the side product formation. However, the pre-standard DIN/TS 51699 (ref. 13) does not limit the concentration of tetroxan. The concentration of TRI is limited to 0.1 wt% and was detected smaller than 0.01

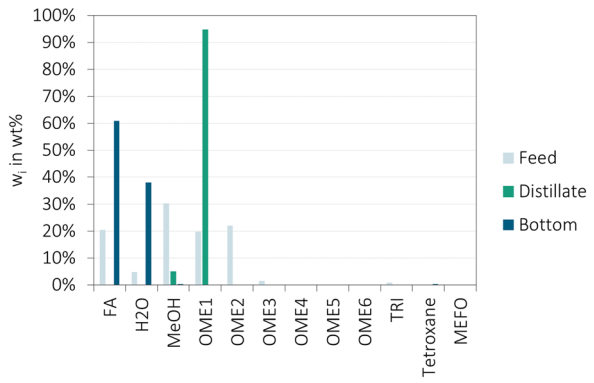

Fig. 8 CO-2, reactive distillation of the distillate product of CO-1 over A46 (conditions: A46/(feed stream) = 0.35 g g^{-1} h^{-1}, 1 L h^{-1}, distillate/feed = 63 wt%, Montz 750 structured packing, 45–104 °C, ambient pressure). The values describe the mass fractions of the feed mixture, the distillate product and bottom product.

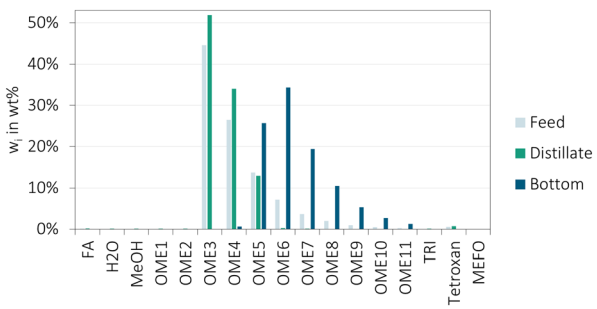

Fig. 9 CO-3, product separation (conditions: 5.5 L h^{-1}, distillate/feed = 82 wt%, Montz 750 structured packing, 100–210 °C, 200 mbar). The values describe the mass fractions of the feed mixture, here the CO-1 bottom product, the distillate product and bottom product.

wt% in the distillate product of CO-3. The final OME_{3-5} product from the COMET process was compatible with the pre-standard DIN/TS 51699.

Due to the solidification of the bottom product $OME_{\geq 5}$ at room temperature, it was diluted in THF with a ratio of 1 : 10 g/g to enable the GC analysis. However, this also impairs the detection limits and accuracy of the analysis. Alternatively, to liquify the bottom product it can also be heated up. At 80 °C, the bottom product is completely liquid, which enables its recycling to the reactor, as illustrated in Fig. 3.

The distillation setup was operated at a condensation temperature of 140 °C and a reboiler temperature of 210 °C. The high distillate temperature was a result of the high feed flow rate and the limited area for condensation. As a result, a complete condensation was not obtained and small fraction of OME_3 accumulated in a cool trap. In contrast to the other distillation experiments the operation pressure was reduced to 200 mbar to reduce the reboiler temperature for the separation between OME_5 and OME_6. The distillate to feed ratio was about 0.82.

5.2. Process simulation and evaluation

5.2.1. Mass balance. Stream compositions and conditions of the COMET process simulation in Aspen Plus are listed in Table 4, following the stream numbering of Fig. 3. Stream compositions and conditions for all sub-processes are presented in the ESI.†

The feedstock (stream 1) containing about 50 wt% FA and 49 wt% H_2O is mixed with the distillate of the second evaporator E-2 and the bottom of the third evaporator E-3. The mixture is concentrated in a cascade of two evaporators E-1 and E-2 operated at 400 and 500 mbar respectively and low retention times. The pressure levels were selected to obtain similar evaporation and condensation temperatures as experimentally verified. However, in practice, the pressure level might be lower to achieve the desired concentrations. This is a result of the simplified modelling of the evaporators which require more detailed considerations of the reaction kinetics of eqn (1)–(4) as recently introduced by Tönges and Burger.[68] The FA concentration is similar to the conventional production of pFA and generates a concentrated FA solution containing about 88 wt% FA (stream 5) and a solution containing about 18 wt% FA (stream 3). Stream 3 is split to be used as a washing liquid for the FA absorber column and to be purified in the distillation column CO-4 operated at 5.5 bar to pure H_2O (stream 4) (<200 ppm FA) and a concentrated FA solution with 44 wt% FA. To prevent the accumulation of MeOH and other impurities in the loop, the concentrated FA solution is sent to another evaporator E-3 operated at ambient pressure. This prepares a by-product of the COMET process with a higher MeOH concentration (stream 2) and a FA solution with a similar composition to the FA feedstock, which is recycled to the evaporator cascade. The by-product (stream 2) has a low FA concentration of about 14 wt%. Furthermore, its mass flow is about 17.6% of the mass flow of the target OME_{3-5} product. This high mass flow is similar to alternative OME_{3-5} production processes using FA(aq.) solution as an intermediate product.[19]

The concentrated FA product (stream 5) is pressurized to about 10 bar, then mixed with the recycle streams containing mainly OME_1 and $OME_{>5}$ (stream 10 and stream 14) and converted to OME in a fixed bed reactor at about 10 bar and 90 °C, over A46 catalyst, as used for the experimental demonstration. The reactor product contains about 20 wt% OME_{3-5}, which is relatively high in comparison to the process based on MeOH and FA(aq.), which has 0 to 15 wt% OME_{3-5} in the reactor product,[39] as presented in Table 8. The reactor product is purified in a first distillation column CO-1 operated at a slight overpressure of 1.8 bar, where $OME_{\geq 3}$ are separated from FA, MeOH, H_2O, OME_{1-2} and a small fraction of OME_3. The slight overpressure improves the separation efficiency and reduces the losses of OME_3 to the distillate product (stream 8) to about 12%. The FA concentration of the

Table 4 Stream compositions and conditions of the COMET process presented in Fig. 3

	Overall mass fractions													
Stream	1	2	3	4	5	6	7	8	9	10	11	12	13	14
T in °C	64.9	30.0	90.0	30.0	90.4	90.0	90.0	81.5	81.0	41.5	117.4	200.5	86.6	194.9
p in bar	1.0	1.0	0.3	1.0	10.3	10.0	10.1	1.8	1.8	1.0	1.0	1.8	0.07	0.07
m in kg h^{-1}	18 509	2203	14 753	7870	22 957	66 666	66 666	51 796	5288	41 330	15 753	14 871	12 490	2380
FA	0.502	0.142	0.184	0.000	0.880	0.303	0.186	0.239	0.000	0.000	0.727	0.000	0.000	0.000
H_2O	0.491	0.778	0.796	1.000	0.120	0.042	0.022	0.028	0.000	0.002	0.268	0.000	0.000	0.000
MeOH	0.007	0.080	0.020	0.000	0.000	0.028	0.100	0.129	1.000	0.045	0.005	0.000	0.000	0.000
OME_1	0.000	0.000	0.000	0.000	0.000	0.591	0.276	0.356	0.000	0.953	0.000	0.000	0.000	0.000
OME_2	0.000	0.000	0.000	0.000	0.000	0.000	0.179	0.230	0.000	0.000	0.000	0.000	0.000	0.000
OME_3	0.000	0.000	0.000	0.000	0.000	0.000	0.107	0.017	0.000	0.000	0.000	0.419	0.499	0.000
OME_4	0.000	0.000	0.000	0.000	0.000	0.000	0.061	0.000	0.000	0.000	0.000	0.271	0.323	0.000
OME_5	0.000	0.000	0.000	0.000	0.000	0.000	0.033	0.000	0.000	0.000	0.000	0.149	0.177	0.000
OME_6	0.000	0.000	0.000	0.000	0.000	0.018	0.018	0.000	0.000	0.000	0.000	0.080	0.000	0.496
OME_7	0.000	0.000	0.000	0.000	0.000	0.009	0.009	0.000	0.000	0.000	0.000	0.042	0.000	0.262
OME_8	0.000	0.000	0.000	0.000	0.000	0.005	0.005	0.000	0.000	0.000	0.000	0.022	0.000	0.136
OME_9	0.000	0.000	0.000	0.000	0.000	0.002	0.002	0.000	0.000	0.000	0.000	0.011	0.000	0.070
OME_{10}	0.000	0.000	0.000	0.000	0.000	0.001	0.001	0.000	0.000	0.000	0.000	0.006	0.000	0.036

Table 5 Overall mass balance for the production of OME_{3-5} following the COMET process and the processes P1 and P4 by Mantei *et al.*[19] The processes were simulated with a capacity of 100 kilotons per annum OME_{3-5}

	COMET	P1	P4
Total input in kg $kg_{OME_{3-5}}^{-1}$	6.60	7.54	8.53
H_2	0.25	0.27	0.21
CO_2	1.82	1.96	2.20
Air	4.53	5.32	5.92
Total output in kg $kg_{OME_{3-5}}^{-1}$	6.60	7.54	8.53
OME_{3-5}	1.00	1.00	1.00
OME_3	0.50	0.43	0.43
OME_4	0.32	0.38	0.36
OME_5	0.18	0.19	0.21
Wastewater	1.03	1.30	1.00
Aq. FA solution	0.18	—	—
Exhaust gas	4.39	5.24	6.54

bottom product (stream 12) is reduced to about 100 ppm. In the third distillation column CO-3 operated at 70 mbar, the main product OME_{3-5} (stream 12) is extracted from the process with about 50 wt% OME_3, 32 wt% OME_4, 18 wt% OME_5 and traces of FA and H_2O in compliance with the pre-standard DIN/TS 51699 specifications. The distillate product (stream 8) of the first distillation column CO-1 is mixed with MeOH (stream 9) and introduced to the reactive distillation column CO-2. This column is operated at ambient pressure. The selection of the pressure level is a compromise between the condensation temperature of the distillate, the reaction kinetics on the catalytic trays and the composition of the azeotropic mixture of OME_1 and MeOH in the distillate. A pressure reduction would favorably improve the azeotropic composition to higher OME_1 concentrations. However, it would also lead to a reduction of the condenser temperature below 41 °C which can lead to more expensive cooling utilities and decelerate the reaction kinetics on the catalytic trays. Increased pressure levels would benefit from higher reaction kinetics due to the higher temperature level on the catalytic trays, but lower OME_1 concentrations in the distillate product. This would decrease the OME_{3-5} selectivity in the OME synthesis reactor and necessarily increase the recycle streams and, therefore, the specific heat demand for product purification. The mixture is separated into the azeotropic mixture of 95 wt% OME_1 and 4.5 wt% MeOH in the distillate (stream 10) and a mixture of 73 wt% FA and 27 wt% H_2O in the bottom (stream 11). A summary of the overall mass balance of the COMET process is listed in Table 5.

Table 6 Overall energy demand for the production of OME_{3-5} following the COMET process and the processes P1 and P4 by Mantei *et al.*[19] The processes were simulated with a capacity of 100 kilotons per annum OME_{3-5}

	COMET	P1	P4
Total input kW h kW^{-1} $h_{OME_{3-5},LHV}^{-1}$			
H_2	1.60	1.70	1.34
Total output kW h kW^{-1} $h_{OME_{3-5},LHV}^{-1}$			
OME_{3-5}	1.00	1.00	1.00
Energy demand kW h kW^{-1} $h_{OME_{3-5},LHV}^{-1}$			
Electricity	0.11	0.09	0.14
LPS, 4 bar	0.09	−0.10	0.24
MPS, 23 bar	0.05	0.30	−0.07
Cooling water	−1.02	−1.05	−0.79
Heat. $T > 250$ °C	—	—	0.19

Table 7 Overall process efficiencies for the production of OME_{3-5} following the COMET process and the processes P1 and P4 by Mantei *et al.*[19] The processes were simulated with a capacity of 100 kilotons per annum OME_{3-5}

	COMET	P1	P4
η_{energy} in %	54.1	50.3	54.4
η_C in %	88.1	81.6	72.5
η_{mass} in %	41.1	38.1	41.4

For the comparison with alternative OME_{3-5} production processes the results from Mantei *et al.*[19] are presented for some selected processes, namely: P1, which produced OME_{3-5} *via* MeOH and a concentrated FA solution (aqueous OME synthesis) feedstock, and P4 which produces OME_{3-5} *via* OME_1 and monomeric FA (anhydrous OME synthesis) feedstock. The processes are described in detail in the ESI† in section 1.4 and 1.5.

The results show that the overall COMET process requires less H_2 than P1 but more H_2 than P4. The difference to P1 is mainly based on the FA concentration sub-process, in which the simulation of this work contains a modified separation of FA from H_2O due to the addition of a distillation column and a third evaporator. This results in a smaller amount of FA, which exits the process in the form of an aqueous FA solution by-product stream (see stream 2 in Fig. 3).

The difference to P4 is mainly based on the advantages of the anhydrous FA synthesis from MeOH which produces H_2 as a by- product which can be separated and recycled to the MeOH sub-process. The lower CO_2 demand of the COMET process in comparison to P1 and P4 is also based on the FA concentration sub-process and the anhydrous FA synthesis. P1 requires more CO_2 due to the higher amount of FA in the by-product stream (see stream 2 in Fig. 3). The lower demand of air of the COMET process is mainly a result of the consideration of smaller purge streams which are oxidized in the combustion sub-process. The oxygen demand for the partial oxidation of MeOH towards FA(aq.) is only slightly lower for the COMET process than for P1.

The composition of the final OME_{3-5} product mixture also shows significant differences. While Mantei *et al.*[19] chose a composition close to the highest yield of OME_{3-5} after the synthesis, the composition in this work was selected to meet the requirements for the pre-standard DIN/TS 51699.

Regarding the wastewater production, the COMET process produces less wastewater than P1 but more wastewater than P4. The difference to P1 is mainly based on the composition of the wastewater. While the simulation of the COMET process produces high-purity wastewater and an aqueous FA solution by-product, Mantei *et al.*[19] considered the aqueous FA solution to be part of the wastewater. The difference to P4 is also explained by the anhydrous FA synthesis.[19]

Table 8 Comparison of various OME_{3-5} production processes based on the results of Held *et al.*,[39] Mantei *et al.*[19] and Schemme *et al.*[43]

	Anhydrous synthesis			Aqueous synthesis			
Feedstock	OME_1 and TRI	DME and TRI	OME_1 and monomeric FA	MeOH and FA(aq.)	OME_1 and FA(aq.) or pFA	MeOH and monomeric FA	COMET
$w_{OME_{3-5}}$ in wt%	5, 34[39] 0, 35[43]	—[a]	5, 29[19]	0, 15[39] 4, 16[19] 0, 14[43]	4, 19[19]	3, 19[19]	0, 20
$Q_{Reboiler}/H_{OME_{3-5}}$ in $kW_{Heat}\ kW_{OME_{3-5}}^{-1}$	7.6%[39] 5.5%[43]	—[a]	15%[19]	47%[39] 39%[19] 78%[43]	26%[19]	48%[19]	35%
$\eta_{energy,overall}$ in %	29–37[39] 22–26[43]	—[a]	27–36[19]	30–36[39] 25–31[19] 24–29[43]	26–32[19]	28–37[19]	28–34
Scale-up potential in the near future	Likely	Unlikely	Unlikely	Less likely	Less likely	Unlikely	Likely

[a] Further investigations and an adjusted process concept are required to estimate the process performance.

The exhaust gas flow is lower for the COMET process than for P1 and P4 which is the result of the smaller purge streams and, therefore, the lower air demand for the combustion.

5.2.2. Energy demand. The specific energy demand and operation conditions for the main process units evaluated by the COMET process simulation are listed in the ESI.†

The summary of the overall energy demand of the COMET process after the heat integration in comparison to P1 and P4 is listed in Table 6.

The different H_2 demands between the COMET process, P1 and P4 directly reflect on the total process energy demand. Furthermore, the electricity demand of the COMET process is higher than for P1 but lower than for P4. Compared to P1, the operation conditions of the phase separators in the MeOH sub-process were adjusted resulting in higher recycling rates and, therefore, higher compression demand. Furthermore, P1 and P4 did not consider the compression demand for the combustion sub-process.[19] The higher electricity demand of P4 is a result of the anhydrous FA synthesis, which requires higher recycle streams in comparison to the partial oxidation of MeOH in P1 and the COMET process.[19]

The demand for low pressure steam (LPS) of the COMET process is higher than the demand of P1 but lower than the demand of P4, which is mainly a result of the heat integration strategies. P1 generates more LPS than it consumes, while P4 and the COMET process show higher demands than generated. However, the demand for medium pressure steam (MPS) is lower for the COMET process. P1 shows a very high demand of MPS, while P4 generates more than it consumes. The MPS demand for the COMET process is significantly lower than for P1. The main consumers of MPS are CO-1 and CO-3 in the OME_{3-5} sub-process. However, MPS is also generated in the MeOH synthesis reactor and the combustion sub-process. While the combustion sub-process generates a similar amount of MPS of about −0.15 kW h kW^{-1} $h_{OME_{3-5},LHV}^{-1}$ comparing P1 and the COMET process, the amount differs for the MeOH reactor with −0.04 and −0.11 kW h kW^{-1} $h_{OME_{3-5},LHV}^{-1}$, respectively. The lower MPS generation of P1 is mainly a result of the inlet temperature to the MeOH reactor. The inlet temperature of P1 is about 185 °C and, therefore, needs to be heated up to the operation temperature of 250 °C using generated MPS and the exothermic heat of the methanol synthesis reactor. The inlet temperature of the COMET process simulation is about 240 °C, which requires a larger heat transfer area but improves the energy efficiency. Furthermore, the demand for MPS of the distillation columns in the OME_{3-5} sub-process differ significantly. P1 requires about 0.32 kW h kW^{-1} $h_{OME_{3-5},LHV}^{-1}$ of MPS for the purification of the OME_{3-5} product stream, while the COMET process requires only 0.20 kW h kW^{-1} $h_{OME_{3-5},LHV}^{-1}$. This is mainly a result of the higher OME_{3-5} yield of the COMET process after the OME synthesis reactor as discussed in the previous section.

The demand for cooling water is similar between P1 and the COMET process but significantly lower for P4.[19] The cooling is required mainly for the temperature level between 90 °C and 30 °C and is, therefore, hardly utilizable for the heat integration of the COMET process. Mantei *et al.*[69] proposed the utilization of heat pumps instead of cooling water and evaluated a significant enhancement potential for the overall energy efficiency.

Only P4 has a demand for heat above 250 °C, due to the endothermic anhydrous FA synthesis.

Regarding the heat demand for the separation of H_2O *via* reactive distillation, the COMET process requires about 1.1 kWh kg^{-1} H_2O at 117 °C. This is based on the assumption that the main target of the reactive distillation column is the separation of H_2O from the loop. Therefore, the heat demand of the reboiler and the feed preheater can be allocated to the amount of H_2O separated from the loop.

5.2.3. Process efficiencies. The summary of the overall process efficiencies of the COMET process after the heat integration is listed in Table 7 and compared with P1 and P4.

The overall energy efficiency of the COMET process is higher than P1 and similar to P4. Mantei *et al.*[19] reported an

efficiency of 49–50% for processes considering the FA(aq.) sub-process. Furthermore, the carbon efficiency is considerably higher than P1 or P4. The low carbon efficiency of P4 is mainly a result of the high CO side-product formation during the anhydrous FA synthesis.[19] While the lower carbon efficiency of P1 is mainly a result of the more efficient H_2O separation of the FA concentration sub-process considered for the COMET process simulation. As a result, the carbon efficiency of P1 could also be increased by adjusting the FA concentration sub-process that can be considered in a future work. The OME_{3-5} yield based on the feedstock H_2 and CO_2 is also higher for the COMET process than for P1 which is also a result of the more efficient H_2O separation of the FA concentration sub-process. The OME_{3-5} yield is similar to P4 since H_2O, formed in the FA(aq.) synthesis, is separated from the process loop, compared to the formation, separation and recycling of H_2 in the anhydrous FA synthesis of P4.

5.2.4. Comparison to alternative OME_{3-5} production processes. To compare alternative OME_{3-5} production process concepts, important performance parameters are listed in Table 8. These performance parameters include the mass fraction of OME_{3-5} before and after the OME reactor $w_{OME_{3-5}}$. Furthermore, the heat demand of the reboiler of the distillation columns and feed preheaters of the OME sub-process $Q_{Reboiler}$ in relation to the OME_{3-5} product mass flow times its LHV $H_{OME_{3-5}}$ is considered. Another key performance parameter is the overall energy efficiency $\eta_{energy,overall}$. This considers the entire process chain starting from H_2O electrolysis and CO_2 *via* the production of the intermediate products towards the target product mixture OME_{3-5}.

Regarding the electricity and heat demand for the H_2O electrolysis and CO_2 preparation, the assumptions from Held *et al.*[39] were considered. For the CO_2 preparation all three scenarios from Held *et al.*[39] were considered, comprising CO_2 from point sources (CPS), post combustion capture (PCC) using mono-ethanol amine scrubbing and direct air capture (DAC). The key assumptions for the expanded system boundary evaluation are summarized in ESI† in Table S28. In addition, the scale-up potential in the near future is qualitatively evaluated. The key performance parameters are based on the results from Held *et al.*,[39] Mantei *et al.*[19] and Schemme *et al.*[43]

Regarding the yield of OME_{3-5} after the reactor as illustrated in Fig. 1, the anhydrous process concepts show far higher OME_{3-5} concentrations than the aqueous process concepts, as indicated by $w_{OME_{3-5}}$. This also reflects on the heat demand for the OME_{3-5} product purification, which is compared based on $Q_{Reboiler}/H_{OME_{3-5}}$. The anhydrous process concepts show significantly lower heat demands for the product purification. Exceptions are the production based on OME_1 and FA(aq.) or pFA and the COMET process, which despite comparatively low yields of OME_{3-5} in the reactor require less heat for the separation of the target product than the other aqueous process concepts. For a consistent basis of comparison, the production of the intermediate products for different OME production processes was considered in the evaluation, indicated by $\eta_{energy,overall}$. The result is a low overall energy efficiency of <40% for all processes, with minor differences between anhydrous and aqueous process concepts. Greater differences were reported between different literature sources, which is especially significant comparing the results for the OME_{3-5} production based on OME_1 and TRI as well as MeOH and FA(aq.) from Held *et al.*,[39] Mantei *et al.*[19] and Schemme *et al.*[43] Those differences are discussed in detail by Mantei *et al.*[19] and mainly result from different heat integration strategies and the simulation procedure. Schemme *et al.*[43] only integrated the heat between individual sub-processes, while Mantei *et al.*[19] and Held *et al.*[39] considered the heat integration between all sub-processes. However, Held *et al.*[39] did use stoichiometric material balances and literature data, while Mantei *et al.*[19] and Schemme *et al.*[43] used the process simulation software Aspen Plus.

Regarding the low overall energy efficiency of all OME_{3-5} production processes, Mantei *et al.*[69] showed the potential of including high temperature heat pumps (HTHP) to lift the temperature of the excess heat streams and, therefore, supply internal heat demands and, in addition, external heat demands. This strategy has the potential to lift the overall energy efficiency above 61% considering heat as a valuable by-product of the process. Besides only small differences in the energy efficiency, the production costs of the OME_{3-5} product also show no significant differences between different production processes.[19,43]

Regarding a sustainable large-scale production of OME_{3-5} in the near future the COMET process and a production based on OME_1 and TRI feedstock show great potential to be scaled up today. However, the latter is comparatively complex, comprising five sub-processes for the production of MeOH, FA(aq.), TRI, OME_1 and OME_{3-5}. A sustainable OME_{3-5} production based on the COMET process on the other hand comprises three sub-processes for the production of MeOH, FA(aq.) and OME_{3-5}. The OME production process based on DME and TRI requires further investigations, mainly due to the high MEFO formation during the synthesis and the low activities for the conversion of DME to OME. A fast scale-up of the processes based on monomeric FA is mainly prevented by the low TRL of the monomeric FA production. Finally, the aqueous process concepts require the separation of H_2O from the loop of the OME_{3-5} sub-process, which is the main bottleneck for a fast scale-up. Various concepts for separating H_2O from the loop were already proposed, and some show promising results, as discussed before and demonstrated in this work for the reactive distillation column. This enables a scale-up for the processes based on MeOH and FA(aq.) and OME_1 and FA(aq.) or pFA. In comparison to the OME_{3-5} production based on OME_1 and TRI, the aqueous process concepts enable a considerable simplification, which typically improves the robustness and therefore feasibility for large-scale application.

6. Conclusion

The COMET process, which solves the challenging H_2O management of aqueous OME processes, was introduced in this work. The process benefits from a simple feedstock preparation, a short process chain from H_2 and CO_2 to OME_{3-5}, a comparatively high OME_{3-5} yield after the reactor, and the possibility of extracting the by-product H_2O from the loop using a state-of-the-art reactive distillation unit.

Other H_2O separation methods, as discussed in the literature, were presented, and their main advantages and hurdles were evaluated quantitatively. The main advantage of the H_2O separation in the COMET process *via* reactive distillation is the scale-up potential and the feasible application in large-scale production plants.

Starting solely from MeOH and FA(aq.) commercial feedstocks, the main COMET process units, comprising all evaporation, reaction and separation process steps, were experimentally demonstrated on a pilot scale. Importantly, the technical feasibility of the reactive distillation column – the heart of the COMET process concept – was demonstrated for a long duration of around 600 h on stream. In addition, the purification of the final OME_{3-5} product was successfully realized with a product compliant with the pre-standard DIN/TS 51699.

The COMET process was simulated and evaluated using Aspen Plus and compared with relevant alternative OME_{3-5} production processes. Therefore, the system boundary was expanded, including H_2 production *via* H_2O electrolysis, CO_2 capture and all intermediate production sub-processes. With an overall energy efficiency of 28–34%, depending on the CO_2 source, the energy demand of the COMET process is similar to the alternative OME_{3-5} production processes, in which overall energy efficiencies were evaluated in the range of 25–36%. Moreover, the COMET process shows a higher carbon efficiency of 88%.

The OME market is limited by the lack of technologically feasible large-scale processes. However, compared to relevant alternative OME_{3-5} production processes, the novel COMET process shows the smallest technological hurdles and can already be demonstrated and scaled up.

Symbols

C [—]	Number of carbon atoms
H [kW]	Energy content based on the LHV
m, $\dot{m}_i$ [kg h^{-1}]	Mass flow rate
p [bar]	Pressure
$\dot{Q}_k$ [kW]	Heat flow
T [K]	Temperature
w_i [wt%]	Mass fraction
W_l [kW]	Electric power
η [%]	Efficiency

Sub- and superscripts

C Carbon
i Reactant, component

Abbreviations

A15	Amberlyst® 15
A46	Amberlyst® 46
CO	Distillation column
COMET	Clean OME technology
DAC	Direct air capture
DME	Dimethyl ether
EGR	Exhaust gas recirculation
EPDM	Ethylene propylene diene monomer
FA	Formaldehyde
FA(aq.)	Aqueous FA solution, formalin
FFKM	Perfluoroelastomer
FOAC	Formic acid
GC-FID	Gas chromatograph equipped with a flame ionization detector
GC-TCD	Gas chromatograph equipped with a thermal conductivity detectors
HF	Poly(oxymethylene) hemiformals
HTHP	High temperature heat pump
HVO	Hydrogenated vegetable oil
IER	Ion exchange resin
LHV	Lower heating value
LPS	Low pressure steam
MEFO	Methyl formate
MeOH	Methanol
MG	Poly(oxymethylene) glycols
MPS	Medium pressure steam
OME	Oxymethylene dimethyl ethers
OME_1	Methylal
pFA	Paraformaldehyde
PTFE	Polytetrafluoroethylene
PtL	Power-to-liquid
PtX	Power-to-X
R	Reactor
S	Separator
THF	Tetrahydrofuran
TRI	Trioxane
TRL	Technology readiness level
WtW	Well-to-wheel

Author contributions

Conceptualization, F. M. and O. S.; methodology, F. M. and C. S.; experimental investigation, F. M., C. S. and O. S.; analytics, F. M., C. S. and H. S.; simulation and evaluation, F. M., A. E., F. F. and A. P.; writing – original draft preparation, F. M.; writing – review and editing, O. S. and M. K.; scientific supervision, O. S.; project administration, O. S. All authors have read and agreed to the published version of the manuscript.

Conflicts of interest

There are no conflicts to declare.

Acknowledgements

Deutsche Bundesstiftung Umwelt (DBU) is gratefully acknowledged for funding the work of Franz Mantei (20018/541). Furthermore, ChemCom Industries B.V. is gratefully acknowledged for funding the investigation and providing the chemicals required for the investigations. Moreover, many thanks to INAQUA Vertriebsgesellschaft mbH for providing the catalyst A46.

References

1 C. Hank, A. Sternberg, N. Köppel, M. Holst, T. Smolinka, A. Schaadt, C. Hebling and H.-M. Henning, *Sustainable Energy Fuels*, 2020, **4**, 2256.
2 IEA, *Hydrogen*, *Paris*, 2022.
3 *Hydrogen*, **https://www.iea.org/fuels-and-technologies/hydrogen**, (last accessed December 2022).
4 *Direct Air Capture*, **https://www.iea.org/reports/direct-air-capture**, (last accessed June 2022).
5 M. Härtl, K. Gaukel, D. Pélerin and G. Wachtmeister, *MTZ worldwide*, 2017, vol. 78, p. 52.
6 A. Omari, B. Heuser, S. Pischinger and C. Rüdinger, *Appl. Energy*, 2019, 1242.
7 P. Dworschak, V. Berger, M. Härtl and G. Wachtmeister, *SAE Int. J. Fuels Lubr.*, 2022, **15**, DOI: **10.4271/04-15-02-0008**.
8 A. D. Gelner, D. Rothe, C. Kykal, M. Irwin, A. Sommer, C. Pastoetter, M. Härtl, M. Jaensch and G. Wachtmeister, *Environ. Sci.: Atmos.*, 2022, **2**, 291.
9 C. Hank, L. Lazar, F. Mantei, M. Ouda, R. J. White, T. Smolinka, A. Schaadt, C. Hebling and H.-M. Henning, *Sustainable Energy Fuels*, 2019, **3**, 3219.
10 S. Voelker, S. Deutz, J. Burre, D. Bongartz, A. Omari, B. Lehrheuer, A. Mitsos, S. Pischinger, A. Bardow and N. von der Assen, *Sustainable Energy Fuels*, 2022, **6**, 1959.
11 S. Deutz, D. Bongartz, B. Heuser, A. Kätelhön, L. Schulze Langenhorst, A. Omari, M. Walters, J. Klankermayer, W. Leitner, A. Mitsos, S. Pischinger and A. Bardow, *Energy Environ. Sci.*, 2018, **11**, 331.
12 IEA, *World Energy Outlook 2022*, Paris, 2022.
13 *Kraft- und Brennstoffe - Polyoxymethylendimethylether (OME) - Anforderungen und Prüfverfahren (DIN/TS 51699:2023-04 - Entwurf)*, Beuth Verlag GmbH, Berlin, 2023, **https://www.beuth.de/de/vornorm-entwurf/din-ts-51699/364871868**, (last accessed March 2023).
14 H. Schelling, E. Ströfer, R. Pinkos, A. Haunert, G.-D. Tebben, H. Hasse and S. Blagov, Method for producing Polyoxymethylene Dimethyl Ethers, *US 20070260094A1*, BASF Aktiengesellschaft, 2007.
15 J. Burger, A novel process for the production of diesel fuel additives by hierarchical design, *Ph.D. Thesis*, University of Kaiserslautern, Kaiserslautern, 2012.
16 J. Burger, M. Siegert, E. Ströfer and H. Hasse, *Fuel*, 2010, **89**, 3315.
17 E. Ströfer, H. Schelling, H. Hasse and S. Blagov, Method for the Production of Polyoxymethylene Dialkylethers From Troxan and Dialkylethers, US007999140B2, 2011.
18 C. F. Breitkreuz, N. Schmitz, E. Ströfer, J. Burger and H. Hasse, *Chem. Ing. Tech.*, 2018, **90**, 1489.
19 F. Mantei, R. E. Ali, C. Baensch, S. Voelker, P. Haltenort, J. Burger, R.-U. Dietrich, N. von der Assen, A. Schaadt, J. Sauer and O. Salem, *Sustainable Energy Fuels*, 2022, **6**, 528.
20 N. Schmitz, E. Ströfer, J. Burger and H. Hasse, *Ind. Eng. Chem. Res.*, 2017, **56**, 11519.
21 J. Burger, N. Schmitz, H. Hasse and E. Ströfer, Process for preparing Polyoxymethylene Dimethyl Ethers from Formaldehyde and Methanol in aqueous solutions, US 2018/0134642 A1, 2018.
22 R. Palkovits, C. H. Gierlich and I. Delidovich, Verfahren zur Trennung von Oxymethylenethern, EP 3 514 134 A1, 2019.
23 C. H. Gierlich, Herstellung von Oxymethylenethern anhand von alternativen Reaktionskonzepten, *Ph.D. Thesis*, Aachen, 2021.
24 G. P. Hagen and M. J. Spangler, Preparation of Polyoxymethylene Dimethyl Ethers by Catalytic Conversion of Formaldehyde Formed by Oxidation of Dimethyl Ether, US 6392102 B1, 2002.
25 T. Qiang, W. Jinfu, W. Tiefeng and Z. Yanyan, Method for Preparing DMM3–5 from Hypercoagulable Polyoxymethylene Dimethyl Ether Component DMM6+ and Dimethoxymethane DMM, CN105152882 A, 2017.
26 N. Schmitz, F. Homberg, J. Berje, J. Burger and H. Hasse, *Ind. Eng. Chem. Res.*, 2015, **54**, 6409.
27 N. Schmitz, J. Burger and H. Hasse, *Ind. Eng. Chem. Res.*, 2015, **54**, 12553.
28 T. Grützner, H. Hasse, N. Lang, M. Siegert and E. Ströfer, *Chem. Eng. Sci.*, 2007, **62**, 5613.
29 M. Drexler, P. Haltenort, U. Arnold and J. Sauer, *Chem. Ing. Tech.*, 2022, **94**, 256.
30 C. F. Breitkreuz, N. Hevert, N. Schmitz, J. Burger and H. Hasse, *Ind. Eng. Chem. Res.*, 2022, **61**, 7810.
31 P. Haltenort, K. Hackbarth, D. Oestreich, L. Lautenschütz, U. Arnold and J. Sauer, *Catal. Commun.*, 2018, **109**, 80.
32 J. Voggenreiter and J. Burger, *Ind. Eng. Chem. Res.*, 2021, **60**, 2418.
33 F. Mantei, S. Kopp, A. Holfelder, E. Flad, D. Kloeters, M. Kraume and O. Salem, *React. Chem. Eng.*, 2023, **8**, 917.
34 I. Bogatykh, T. Osterland, H. Stein and T. Wilharm, *Energy Fuels*, 2020, **34**, 3357.
35 K. Hackbarth, P. Haltenort, U. Arnold and J. Sauer, *Chem. Ing. Tech.*, 2018, **90**, 1.
36 H. Liu, Z. Wang, Y. Li, Y. Zheng, T. He and J. Wang, *Appl. Energy*, 2019, **233-234**, 599.
37 D. Bongartz, L. Doré, K. Eichler, T. Grube, B. Heuser, L. E. Hombach, M. Robinius, S. Pischinger, D. Stolten, G. Walther and A. Mitsos, *Appl. Energy*, 2018, 757.
38 D. Bongartz, J. Burre and A. Mitsos, *Ind. Eng. Chem. Res.*, 2019, **58**, 4881.
39 M. Held, Y. Tönges, D. Pélerin, M. Härtl, G. Wachtmeister and J. Burger, *Energy Environ. Sci.*, 2019, **12**, 1019.
40 C. F. Breitkreuz, M. Dyga, E. Forte, F. Jirasek, J. de Bont, J. Wery, T. Grützner, J. Burger and H. Hasse, *Chem. Eng. Process.*, 2021, 108710.
41 J. Sauer and G. Emig, *Chem. Eng. Technol.*, 1995, **18**, 284.

42 J. Burre, D. Bongartz and A. Mitsos, *Ind. Eng. Chem. Res.*, 2019, **58**, 5567.
43 S. Schemme, J. L. Breuer, M. Köller, S. Meschede, F. Walman, R. C. Samsun, R. Peters and D. Stolten, *Int. J. Hydrogen Energy*, 2020, **45**, 5395.
44 P. Haltenort, L. Lautenschütz, U. Arnold and J. Sauer, *Top. Catal.*, 2019, **62**, 551.
45 M. Drexler, P. Haltenort, U. Arnold, J. Sauer, S. A. Karakoulia and K. S. Triantafyllidis, *Catal. Today*, 2022, 113847.
46 X. Li, J. Cao, M. A. Nawaz, Y. Hu and D. Liu, *J. Chem. Eng. Data*, 2019, **64**, 5548.
47 X. Li, H. Tian, W. Zhang and D. Liu, *International Journal of Chemical and Molecular Engineering*, 2018, 536.
48 L. Wang, S. Zhou, P. Li, P. Li, Q. Li and Y. Yu, *J. Chem. Eng. Data*, 2018, **63**, 3074.
49 M. Shi, X. Yu, G. He and Q. Li, *Can. J. Chem. Eng.*, 2018, **96**, 968.
50 M. Shi, G. He, F. Gan, X. Yu and Q. Li, *J. Chem. Eng. Data*, 2017, **62**, 2183.
51 Z. Zhuang, J. Zhang and D. Liu, *Huagong Xuebao*, 2016, **67**, DOI: **10.11949/j.issn.0438-1157.20160391**.
52 Z. Zhuang, J. Zhang, X. Liu and D. Liu, *J. Chem. Thermodyn.*, 2016, 190.
53 D. Oestreich, L. Lautenschütz, U. Arnold and J. Sauer, *Fuel*, 2018, **214**, 39.
54 A. Ferre and J. Burger, *Ind. Eng. Chem. Res.*, 2021, **60**, 15256.
55 S. Schemme, Techno-ökonomische Bewertung von Verfahren zur Herstellung von Kraftstoffen aus H2 und CO2, *Ph.D. Thesis*, Aachen, 2020.
56 N. Schmitz, Production of poly(oxymethylene) dimethyl ethers from formaldehyde and methanol, *Ph.D. Thesis*, Scientific Report Series, Kaiserslautern, 2018.
57 N. Schmitz, C. F. Breitkreuz, E. Ströfer, J. Burger and H. Hasse, *J. Membr. Sci.*, 2018, **564**, 806.
58 A. Ferre, J. Voggenreiter, Y. Tönges and J. Burger, *Motortech. Z.*, 2021, **82**, 28.
59 F. Mantei, M. Ouda and A. Schaadt, Method for Producing Polyoxymethylene Dimethyl Ethers, WO22013132 A1, 2022, **https://worldwide.espacenet.com/patent/search/family/077168217/publication/WO2022013132A1?q=pn%3DWO2022013132**, (last accessed July 2022).
60 *Ullmann's Encyclopedia of Industrial Chemistry: Formaldehyde*, ed. A. W. Franz, H. Kronemayer, D. Pfeiffer, R. D. Pilz, G. Reuss, W. Disteldorf, A. O. Gamer and A. Hilt, Wiley-VCH Verlag GmbH & Co. KG, Weinheim, 2016.
61 J.-O. Drunsel, Entwicklung von Verfahren zur Herstellung von Methylal und Ethylal, *Ph.D. Thesis*, Scientific Report Series, Kaiserslautern, 2012.
62 H. Hasse, J.-O. Drunsel, J. Burger and U. Schmidt, Process for the production of pure Methylal, WO 2012/062822 A1, 2012.
63 I. Bogatykh, T. Osterland, H. Stein and T. Wilharm, *Energy Fuels*, 2019, **33**, 11078.
64 Kontinuierliche Destillation PD250 AD, **https://asg-analytik.de/technikum/z1-sp2/glaskolonnen**, (last accessed February 2023).
65 A. Fink, C. H. Gierlich, I. Delidovich and R. Palkovits, *ChemCatChem*, 2020, **12**, 5710.
66 A. Fink, Struktur-Aktivitätsbeziehungen von Zeolithen als feste Säurekatalysatoren in der Synthese von Oxymethylendimethylethern, *Ph.D. Thesis*, Aachen, 2022.
67 C. J. Baranowski, A. M. Bahmanpour and O. Kröcher, *Appl. Catal., B*, 2017, **217**, 407.
68 Y. Tönges and J. Burger, *Chem. Eng. Res. Des.*, 2022, **189**, 572.
69 F. Mantei, M. Kraume and O. Salem, *Chem. Ing. Tech.*, 2022, **25**, 912.